Towards room temperature operation of all-solid-state Na-ion batteries through polyester–polycarbonate-based polymer electrolytes

Keywords

All-solid-state batteries, solid polymer electrolyte, room temperature cycling, sodium-ion

Abstract

In an ambition to develop solid-state Na-ion batteries functional at ambient temperature, we here explore a novel electrolyte system. Polyester-polycarbonate (PCL–PTMC) copolymers were combined with sodium bis(fluorosulfonyl)imide salt (NaFSI) to form solid polymer electrolytes for Na-ion batteries. The PCL–PTMC:NaFSI system demonstrated glass transition temperatures ranging from −64 to –11 °C, increasing with increasing salt content from 0 to 35 wt%, and ionic conductivities ranging from 10^{-8} to 10^{-5} S cm^{-1} at 25 °C. The optimal salt concentration was clearly dependent on the level of crystallinity, which was largely determined by the CL content. At 70 and 80 mol% CL, the PCL–PTMC:NaFSI system was fully amorphous and exhibited high conductivities at lower salt concentrations. When the CL content was increased to 100 mol%, high ionic conductivities were instead observed at high salt concentrations. A decent transference number of ca. 0.5 at 80 °C was obtained for a polymer film containing 20 mol% CL units and 25 wt% NaFSI. Finally, a HC|80-20_{25}|$Na_{2-x}Fe(Fe(CN)_6)$ all-solid-state polymer electrolyte full cell was assembled to demonstrate the practical application of the material and cycled for more than 120 cycles at ~22 °C.

1. Introduction

The recent surge of electric vehicles and consumer electronics powered by lithium-ion batteries (LIBs) has brought attention to potentially dangerous design flaws. These are generally associated with the flammability of the liquid electrolyte which, together with the desire to further increase the energy storage per unit volume, has compounded risks of thermal runaway accidents.[1,2] Common strategies to mitigate this safety risk include integrated sensors, pressure release valves, cooling systems and reinforced battery packs.[3] As a result, the overall weight, price, and complexity of the already cumbersome battery pack system increases. Another alternative is to replace the liquid electrolyte with a non-volatile solid polymer electrolyte (SPE), and thereby eliminating the need for the aforementioned safeguards. Ceramic electrolytes are also a promising option in this context, but SPEs have the upper hand in terms of scalability and electrode–electrolyte wettability and are thus highly relevant options despite their relatively low ionic conductivity at ambient temperature. Another argument in favor of SPEs, perhaps less discussed in scientific literature, is the inability of ceramic electrolytes to accommodate volumetric changes occurring in the electrodes during redox activity without compromising electrochemical contact. This inevitably leads to capacity fading.[4]

Safety is not the sole concern for the advancement of batteries as energy storage devices in the future energy system, but it has also become evident that relying solely on a narrow collection of battery chemistries for mobile and stationary applications is a not only an economically risky strategy, but also environmentally less sustainable.[5] This calls for a diversification of available alternative secondary battery chemistries, where not least sodium-ion batteries (SIBs) are foreseen a prosperous future.[6] Sodium shares many electrochemical properties with lithium and would not require extensive changes to battery architecture.

Contrary to lithium, sodium is an abundant resource and does not alloy with aluminum,[6] which means that aluminum current collectors can be used on the anode side instead of copper, which is more expensive and heavy. In the context of polymer electrolytes, the slightly different properties of the Na^+ ion – larger atomic radius, lower charge density, and weaker interaction with anions and larger complexes – may favor the segmental motion mechanism which is responsible for ion transport in polymer electrolytes.[7] Moreover, the solid electrolyte interphase (SEI) in SIBs is much more prone to dissolution over time than the SEI in LIBs.[8] Implementation of SPEs, with comparatively weak dissolving properties, may prove to be an effective strategy to mitigate this.

Among solvent-free polymer electrolyte alternatives (*i.e.*, SPEs), most studies have focused on poly(ethylene oxide) (PEO),[9–17] which typically requires temperatures exceeding 60 °C to function properly.[7] Consequently, no one has managed to construct a full-cell SPE-based SIB that can function at room temperature. Instead, all of the SPE-based SIBs demonstrated so far have been half-cells; *i.e.*, employing a sodium metal anode, usually operating at elevated temperatures.[9,10,18,19,11–16,20–22] Using a sodium metal anode is problematic for primarily two reasons; firstly, sodium metal is highly reactive and quickly forms an oxide if not handled under strictly inert conditions (*i.e.* in an argon glovebox). Replicating this requirement on a large scale is simply too expensive compared to a dry room. Secondly, sodium metal melts at 98 °C which means that the temperature of the battery cannot exceed ~90 °C. This puts large demands on cooling and heating to stay within the operating window of PEO. Furthermore, from an analytical perspective, opting for a full-cell configuration means that the cathode active material provides the sole source of sodium. Without an almost infinite supply of sodium, which is the case when employing a sodium metal electrode, full cells cannot replenish capacity fade and thus give a more accurate depiction of how much sodium is lost to

potential SEI formation or other parasitic side-reactions. To our knowledge, the only existing example of an all-solid-state polymer electrolyte SIB full cell was reported by Ma *et al.* more than 25 years ago: a $Na_{15}Pb_4$|PEO:NaTf|$Na_{0.7}CoO_2$ cell was cycled at 100 °C for an impressive 190 cycles, but the capacity utilization never exceeded 60 % and the cell displayed capacity fading over time.[17] Thus far, none have reported a full-cell all-solid-state SPE-based SIB capable of operating at room temperature.

As an alternative to the popular ether-based electrolytes, Mindemark *et al.* synthesized a polycaprolactone–polytrimethylene carbonate (PCL–PTMC) copolymer with LiTFSI.[23] Optimal performance was attained when the molar ratio was 80:20 polycaprolactone:polycarbonate. The material exhibited a respectable total ionic conductivity of 4.1×10^{-5} S cm^{-1} at 25 °C and a high cation transference number of 0.62 at 40 °C, much higher than previously reported for PEO systems.[24,25] The PCL–PTMC owes its performance to the tuned balance of the flexible caprolactone units and the amorphous phase which is obtained when the trimethylene carbonate units disrupt the PCL crystallinity.[26] In comparison to PCL–PTMC, PEO has a higher degree of crystallinity at room temperature and it forms stronger complexation with the cations, circumstances which are known to hamper ion transport.[15,16,25] The practical application of the PCL–PTMC material was also demonstrated in a $LiFePO_4$ half-cell, which was cycled at ~23 °C.[23]

In this current study, we explore if the PCL–PTMC host matrix is similarly applicable to an SIB system. In order to determine the optimal composition and comprehend the effects of introducing sodium instead of lithium on total ionic conductivity and glass transition temperature in the PCL–PTMC system, different samples of varying salt concentration and PCL content were synthesized and then analyzed using a range of field-standard techniques.

Finally, the material was assembled in a full cell consisting of a hard carbon anode and a Prussian blue cathode and cycled at 40 °C and room temperature to demonstrate its practical application in a SIB.

2. Results & discussion

2.1. Thermal properties

In SPEs, where ionic mobility is strongly coupled to polymer segmental motion, a low T_g is generally recognized as a necessity for fast ion transport and is therefore often cited as an initial indicator to gauge whether or not a polymer is a suitable ion-conductive medium. It is for example one of the primary reasons why PEO long has dominated the field of polymer electrolytes; PEO (without salt) has a relatively low T_g of approximately −60 °C.[25] In this work, the thermal properties of the PCL–PTMC system was studied using DSC and the obtained heating scans can be seen in Figures S1 to S4 in the Supplementary Information. Henceforth, the different electrolytes will be abbreviated as the following examples: PCL_{80}-$PTMC_{20}$ + 25 wt% NaFSI will be denoted as $80\text{-}20_{25}$ and the PCL_{80}-$PTMC_{20}$ system will be denoted as 80-20. As seen in the scans, no melting peaks were observed for 70-30 and 80-20 for all salt concentrations whilst 90-10 and 100-0 exhibited semi-crystallinity, only becoming amorphous at salt concentration above 25 or 35 wt%. The tendency of 90-10 and 100-0 to form semi-crystalline films was also confirmed visually as the films were slightly opaque and milky in appearance. This is expected, considering that the same behavior was seen in the PCL–PTMC:LiTFSI system.[23]

As seen in Figure 1, the T_g for all compositions increased with increasing NaFSI salt concentration. This is attributed to cross-linking effects between the cations and the coordination sites on the polymer chains resulting in lower segmental mobility of the polymer chains.[27,28] Without the addition of salt, the T_g ranges from −64 °C for 100-0 to −55 °C for 70-

30 and the T_g can also be correlated to the portion of PTMC in the copolymer. This is expected since the T_g of PTMC is higher compared to the T_g of PCL (−15 °C and −60 °C, respectively).[25,29] At 10 wt% salt, 70-30 and 80-20 are completely amorphous, see Figures S1 to S4 in the Supplementary Information. 90-10 and 100-0, on the other hand, still maintain some degree of crystallinity most likely because 90-10 and 100-0 contain more PCL and therefore require more salt to fully suppress crystallization. At salt concentrations ranging from 10 to 25 wt%, the relationship between T_g and polymer electrolyte composition becomes seemingly more complex. This can be explained by a series of competing phenomena in the co-existing amorphous and crystalline phases, *e.g.*, the plasticizing effect of the FSI anion, ion–polymer interactions inhibiting segmental motion, and suppression of crystallinity. At 35 wt% NaFSI, the T_g ranges from −24 °C for 100-0 to −11 °C for 70-30 and as previously mentioned, it is at this salt concentration that all of the polymer compositions are completely amorphous. In this regime, the T_g once again becomes directly dependent on the portion of PTMC in the copolymer.

In the preceding work on the PCL–PTMC system involving LiTFSI salt instead of NaFSI, Mindemark *et al.* reported a T_g ranging from −50 °C to −36 °C for 80-20_{20} to 80-20_{36}, respectively.[23] This T_g range is lower in comparison to the PCL–PTMC:NaFSI system where the T_g ranged from −49 °C and −16 °C for 80-20_{10} and 80-20_{35}, respectively, despite lower NaFSI salt concentrations. This could be attributed to the larger radius of Na^+ as compared to Li^+, which would allow higher coordination numbers, leading to a larger degree of stiffening of the system. A similar effect on the T_g can be observed when comparing NaTFSI and LiTFSI salts in pure PTMC.[21,30] In other words, the effect of physical cross-linking becomes stronger for Na^+ in the polyester–polycarbonate host. Higher coordination numbers for Na^+ compared to Li^+ have been shown through DFT calculations, in for example PEG (which is chemically equivalent to PEO).[31] Another possible explanation which can contribute is the

plasticizing effect of the bulkier TFSI anion. For example, the increase in T_g reported for PTMC:NaFSI was higher compared to the T_g range reported for PTMC:NaTFSI.[21,32] If T_g would provide a strong indicator of conductivity performance, it could be concluded that switching to NaFSI from LiTFSI is not obviously favorable for the PCL–PTMC system.

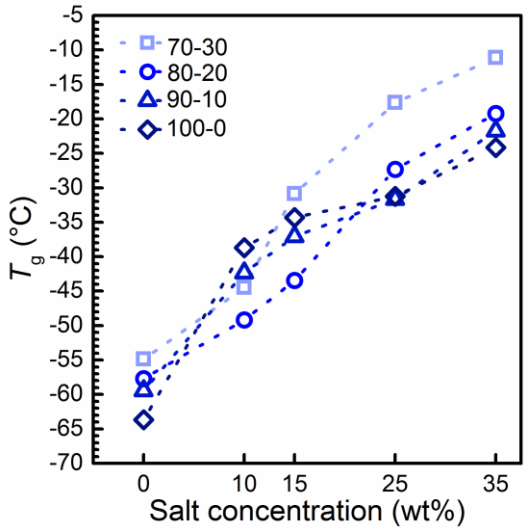

Figure 1: The effect of salt concentration on glass transition temperature, T_g, for the PCL–PTMC system with different concentrations of NaFSI salt.

2.2 Total ionic conductivity

The total ionic conductivity at different temperatures for the PCL–PTMC:NaFSI system was mapped using electrochemical impedance spectroscopy and can be seen in Figure 2. All compositions except 100-0 exhibited Vogel–Fulcher–Tammann (VFT) behavior as seen by the dashed lines in Figure 2 (fitted values can be found in the supplementary information, see Table S1). This indicates that the ionic conductivity is indeed dependent on the segmental motion of the polymers in the amorphous phase. For the semi-crystalline 100-0 material, it was not until temperatures exceeded the melting point of polycaprolactone (~58 °C, see Figure 4 in Supplementary Information) or when the salt content was 25 wt% or above, that conductivity behavior reminiscent of VFT could be observed. A similar behavior was observed by Eriksson *et al.* in the pure PCL system with LiTFSI salt concentrations ranging

from 9 to 30 wt%.[33] The ionic conductivities of the semi-crystalline 100-0 ranged from 7.25×10^{-8} to 1.64×10^{-5} S cm^{-1} at 25 °C for 100-0_{10} and 100-0_{35}, respectively. As mentioned in the experimental section, the 100-0 has a significantly lower molecular weight compared to the other copolymers. This should, however, not affect the ionic conductivity significantly, since the PCL is still macromolecular. For example, for PEO it has been shown that the ionic conductivity remains fairly constant once the molecular weight exceeds 10 000 g mol^{-1}.[34,35] It should be stressed that an unfortunate disadvantage of the 100-0 material at this molecular weight is that it loses useful mechanical stability at temperatures above its melting point, as well as when the salt concentration exceeds 25 wt%.

Overall, the highest ionic conductivity observed at 25 °C was 1.28×10^{-5} S cm^{-1} for the amorphous 80-20_{10}. This is on par with the conductivity previously reported for the PCL–PTMC:LiTFSI system (4.1×10^{-5} S cm^{-1} at 25°C for 80-20_{35}) and far superior compared to the to the value reported for the PEO:NaFSI system (~10^{-7} S cm^{-1}).[23,16] At 80 °C, the conductivity for 80-20_{35} was 0.33 mS cm^{-1} which is merely *ca.* one order of magnitude less than the ionic conductivity reported for conventional liquid Na-ion battery electrolytes: ~6.85 mS cm^{-1} at 25 °C for 0.6 M $NaPF_6$ in EC:DMC.[36]

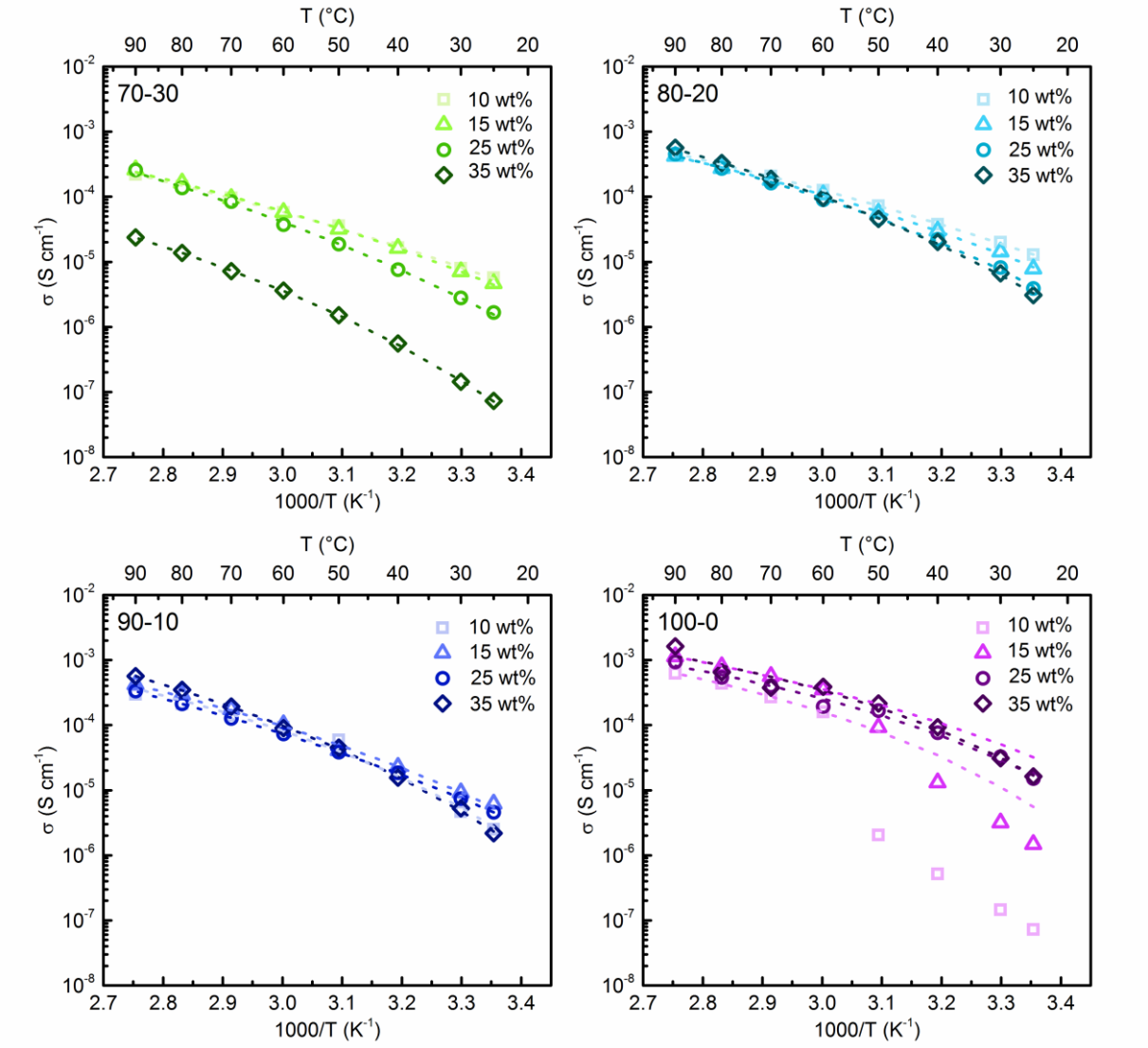

Figure 2: Total ionic conductivity as a function of temperature for PCL_{100-x}-$PTMC_x$ (x=0, 10, 20, and 30) with different NaFSI salt concentrations. Dashed lines represent VFT fitting over the temperature interval in which the polymers are amorphous and extrapolated below T_m for the semi-crystalline materials. Fitted VFT parameters can be found in Table S1.

Based on the surmise that a low T_g is desirable for high ionic conductivity, one would expect that PCL–PTMC compositions with a lower salt concentration would exhibit optimal conductive properties. As seen in Figure 2 and 3a, the statement clearly holds true for the 70-30 and 80-20 (although not very pronounced) at room temperature. As the salt concentration increases from 10 to 35 wt%, the T_g steadily increases and the ionic conductivity drops from

approximately 10^{-5} to 10^{-6} S cm^{-1}; see Figure 3a. This indicates that the cross-linking effect becomes the chief determining factor in terms of ionic conductivity, despite the increased number of charge carriers. 100-0, on the other hand, exhibits the reverse behavior: the relationship between T_g and ionic conductivity has a positive correlation at room temperature. As previously mentioned, the salt suppresses crystallinity, thereby creating larger amounts of the conductive amorphous domains. Although the T_g increases slightly, there is thus still an increase in ionic conductivity. The semi-crystalline 90-10 exhibits an interesting conductivity behavior, which is reminiscent of the behavior shown by both the amorphous and crystalline compositions. For all electrolytes, once the operational temperature exceeds the melting point of PCL, the impact of PCL–PTMC ratio and salt concentration becomes less evident; see Figure 3b.

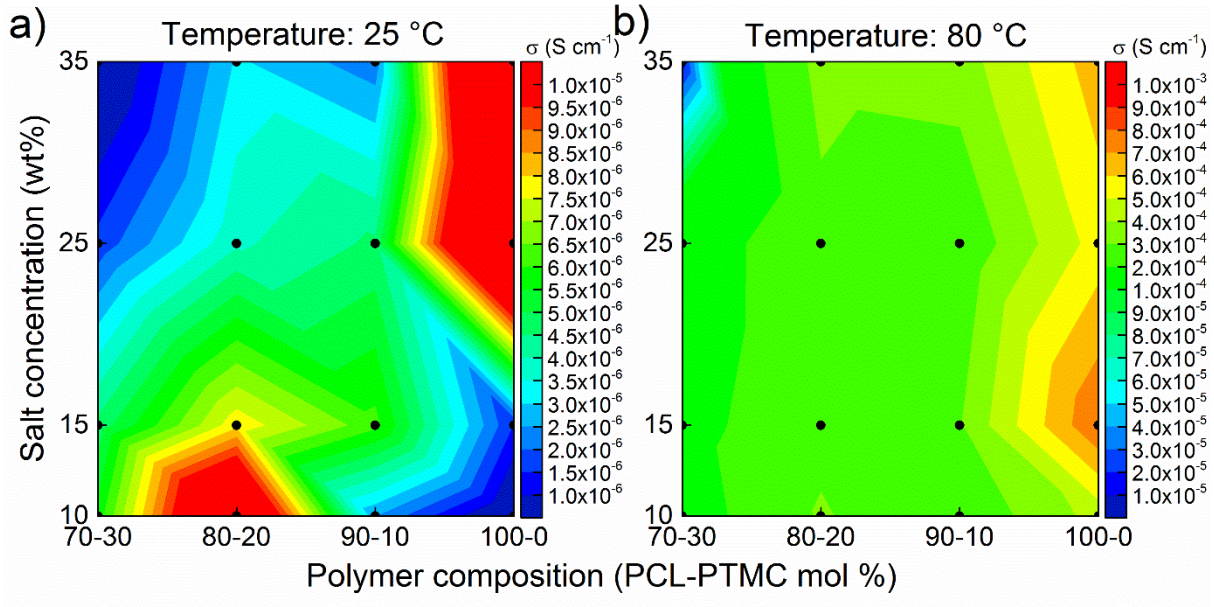

Figure 3: Total ionic conductivity isotherms at (a) 25 °C and (b) 80 °C for the PCL–PTMC:NaFSI system. Measurements points are indicated by black dots; exact values can be seen in Table S2. Note that the conductivity scales differ in a) and b).

2.3 Transference number

Total ionic conductivity, albeit an important parameter, has its limitations since it does not differentiate between cationic and anionic contributions to ionic transport. Thus, a separate technique developed by Bruce and Vincent is commonly employed to determine what fraction of the current is carried by the cations relative to the anions, also known as the transference number (T^+).[37] Ideally, an electrolyte in an LIB or SIB has a T^+ equal to unity, *i.e.* the current is only carried by the cations.

Switching from lithium to sodium may be advantageous or disadvantageous for the transference number, and may also depend on the polymer host; either the lower charge density results in a weaker coordination interaction and thereby facilitates easier movement, or the larger ionic radius can accommodate more coordination sites to wrap around the cation, thereby impeding ion movement.[7] The latter seems to be the case in PCL–PTMC. Inserting values obtained from potentiostatic polarization (Figure 4) into the Bruce–Vincent equation yields a T^+ of 0.47 for 80-20_{25} at 80 °C (see Supplemetary Information for values and calculations). This is comparatively lower than the $T^+ = 0.66$ observed for the 80-20 copolymer with 36 wt% LiTFSI at 60 °C.[23] Interestingly, the same scenario seems to apply to the PTMC system where the transference number reported for $PTMC_5$NaFSI (equivalent to 29 wt% NaFSI) was 0.48 at 80 °C, compared to 0.8 at 60 °C reported for $PTMC_8$LiTFSI.[30,32] Another possible factor which may influence the higher transference number observed for the Li-based SPE is the presence of a bulkier salt anion, in that case TFSI, which likely possesses lower mobility than the smaller FSI anion.

To compare with PEO, transference numbers of 0.15 (with $NaClO_4$) and 0.16 (with NaFSI) have been reported.[15,16] This is comparable with values reported for the LiTFSI analogues which typically range between 0.1 to 0.2.[38] As mentioned in the introduction, PEO strongly coordinates the cation through chelation using multiple oxyethylene groups adjacent along the same polymer chain. This makes PEO effective at dissolving salts, but the very same

mechanism also hampers the release of these cations during segmental motion. As a result, the cationic transference numbers are typically low, and other polymer hosts may provide an improvement.[25]

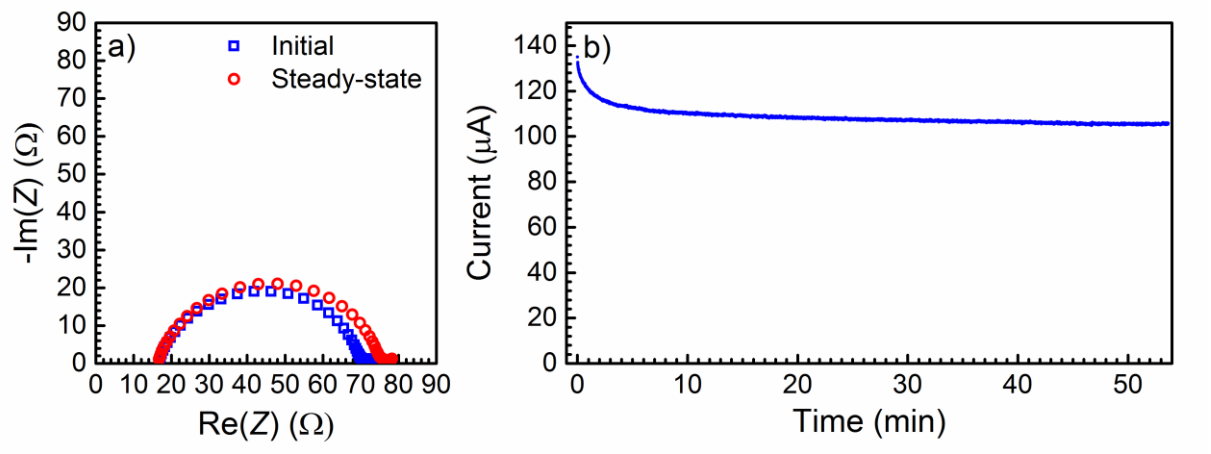

Figure 4: Determination of the transference number for 80-20_{25}. a) Nyquist plot of initial and steady-state impedance response before and after potentiostatic polarization at 80 °C. b) Current relaxation during potentiostatic polarization at 80 °C.

2.4 Cycling of all-solid-state sodium-ion batteries As mentioned in the introduction, few have illustrated the practical application of solid-state polymer electrolytes in Na-ion full-cell format, and none have demonstrated functional operation at ambient temperature. In this work, the 80-20_{25} electrolyte was assembled together with a hard carbon (HC) anode and a Prussian blue ($Na_{2-x}Fe[Fe(CN)_6]$) cathode and cycled at both 40 °C and ambient temperature (~22 °C), see Figure 5 and 6. 80-20_{25} did not have the highest ionic conductivity in the PCL–PTMC:NaFSI system (3.9×10^{-6} S cm^{-1} at 25 °C compared to 1.28×10^{-5} S cm^{-1} at 25 °C for 80-20_{10}); however, the combination of ionic conductivity, high concentration of charge carriers, excellent wetting ability due to its adhesive character, complete amorphicity, and superior mechanical stability compared to 80-20_{10}, 90-10_{25} and 100-0_{25}, made it the prevailing choice.

At 40 °C, the total ionic conductivity of 80-20_{25} (2.23×10^{-5} S cm^{-1}) is one order of magnitude higher than the conductivity at 25 °C. This made it possible to cycle the cell at different current densities ranging from 10 to 120 µA cm^{-2} without suffering severe capacity drop, see Figure 5a. As seen in Figure 5b, the first charge curve shows two distinct plateaus at about 2.5 and 3.2 V which correspond to the oxidation of the high- and low-spin Fe^{II}/Fe^{III} redox couples in $Na_{2-x}Fe[Fe(CN)_6]$.[39,40] Assuming a specific capacity of 234 mAh g^{-1} for hard carbon and a specific cathode capacity of 155 mAh g^{-1}, the active mass loading was balanced with a 1:1 capacity ratio for the anode and the cathode (the cathode and anode mass loading being 3.04 and 1.84 mg cm^{-2}, respectively). Despite no attempts to improve the electrolyte–electrode contact after assembly (no annealing or rest period prior to cycling), the initial charge capacity was 155 mAh g^{-1} based on mass of the cathode active material. If it is assumed that all the capacity was generated by the de-intercalation of Prussian blue, then it strongly indicates complete infiltration of the porous electrode by the soft-matter electrolyte. The cell exhibited capacity fading, with the capacity reaching 70 mAh g^{-1} after 25 cycles. This phenomenon was also observed in a liquid electrolyte benchmark cell (see Figure S6a) and is a common problem associated with hard carbon anodes, and therefore likely not associated with the polymer electrolyte material.[41]

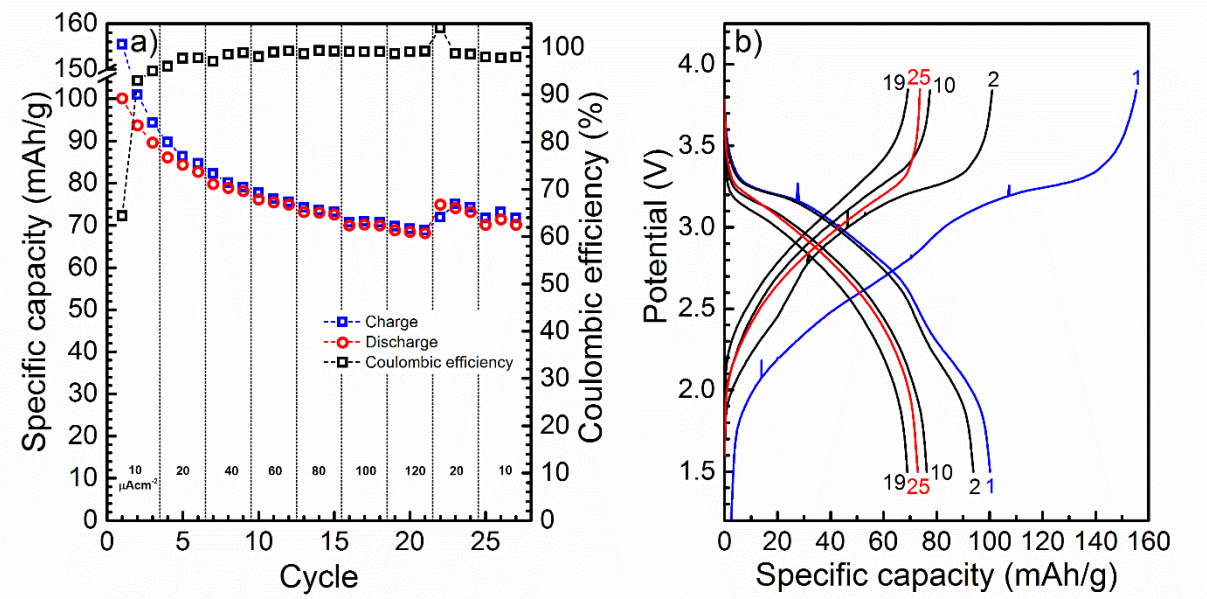

Figure 5: a) Charge and discharge capacity and Columbic efficiency per cycle and b) Voltage profiles, for HC|80-20$_{25}$|Na$_{2-x}$Fe(Fe(CN)$_6$) cycled at 40.0 °C.

Finally, the polymer electrolyte material was pushed towards its low-temperature limits and cycled at ambient temperature, something not possible using PEO-based electrolytes. In order to realize low-temperature cycling, the mass loading of the cathode composite was halved, *i.e.* 1.61 mg cm^{-2} (the anode mass loading was kept constant), which resulted in a capacity ratio of 1:2 for the cathode versus anode. Despite the unbalanced capacity ratio, the initial charge capacity was 140 mAh g^{-1}, which is merely 10 % less than the expected 155 mAh g^{-1}. Similarly to the cell shown in Figure 5, the cell demonstrated capacity fading with time, again likely due to irreversible capacity loss on the hard carbon anode. After approximately 28 cycles, the cell exhibited unstable coulombic efficiencies which seems to indicate the onset of side-reactions. We have previously demonstrated stable cycling of a Na|PTMC:NaFSI|(Na$_x$Fe[Fe(CN)$_6$]) cell which cycled for 80 consecutive cycles with an average discharge capacity of 90 mAh g^{-1} at 60 °C.[32] By the process of elimination, this indicates that the culprit in the HC|80-20$_{25}$|Na$_{2-x}$Fe(Fe(CN)$_6$) cell is either the addition of the

PCL component, or a parasitic reaction taking place in the presence of hard carbon. Despite this, the PCL–PTMC:NaFSI material allowed us to achieve low-temperature cycling for more than 120 cycles. To our knowledge, this has not been achieved before. Doeff *et al.* published a series of studies among which they demonstrated thin-film half-cells with a PEO:$NaCF_3SO_3$ polymer electrolyte operating at 85 °C for 60 cycles.[13,14] More recent examples include the work by Colò *et al.*, who showcased a Na|PEO:$NaClO_4$|$NaFePO_4$ cell operating for 20 cycles at 60 °C and Qi *et al*. demonstrated a Na|PEO:NaFSI|$Na_{0.67}Ni_{0.33}Mn_{0.67}O_2$ cell cycling for 30 cycles at 80 °C.[15,16]

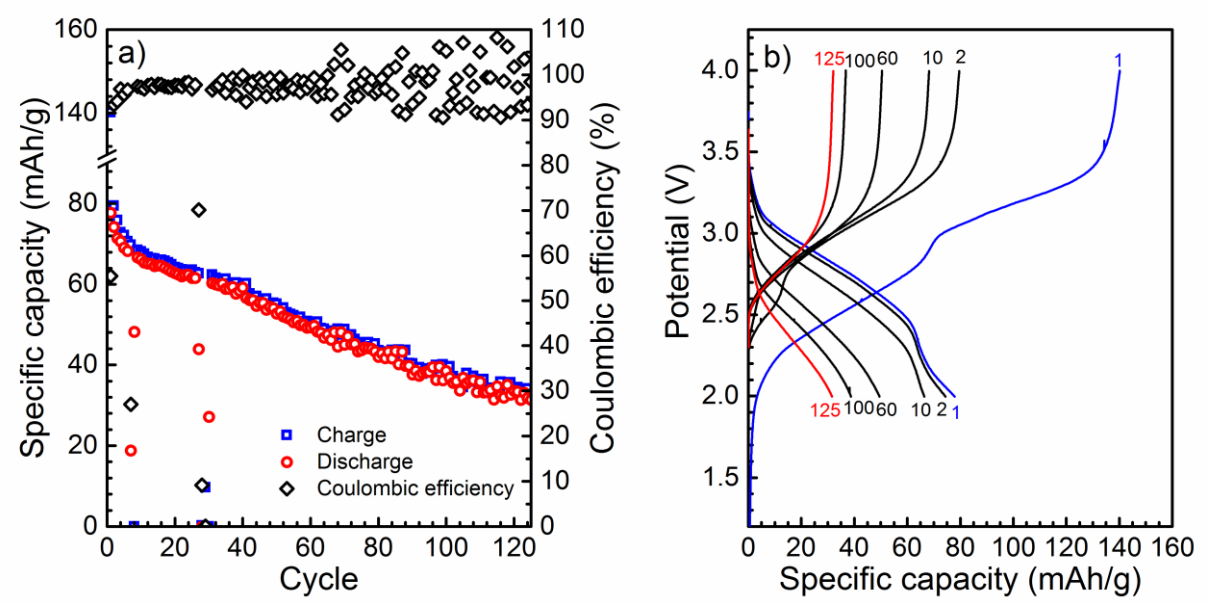

Figure 6: a) Charge and discharge capacity and coulombic efficiency per cycle and b) voltage profiles for HC|80-20_{25}|$Na_{2-x}Fe(Fe(CN)_6)$ cycled at ~22 °C and 10 µA cm^{-2}.

3. Conclusion

We have in this study investigated electrolytes based on NaFSI dissolved in the polycaprolactone–poly(trimethylene carbonate) copolymer system. While increasing salt content generated an expected increase in glass transition temperature, a low glass transition temperature did not directly translate into high ionic conductivity. Instead, the amorphous 70-

30 and 80-20 electrolytes exhibited higher ionic conductivities at the lower end of the salt spectrum, while the semi-crystalline 100-0 exhibited the opposite behavior. This was attributed to the decreasing crystallinity in 100-0 as the salt concentration increased. Interestingly, a significant increase in glass transition temperature and subsequent decrease in total ionic conductivity as well as transference number was observed relative to values reported for the analogous lithium system. This indicates that the larger ionic radius of the sodium ion compared to lithium allows for more carbonyls to coordinate the cation thereby stiffening the system and hampering ionic transport. Overall, conductivity maxima above 10^{-5} S cm^{-1} were observed at 25 °C and a cationic transference number of ca. 0.5 at 80 °C, enabling room temperature cycling of all-solid-state SIBs comprising SPEs. Accordingly, the practical application of polycaprolactone–poly(trimethylene carbonate) polymer electrolytes was demonstrated by assembling all-solid-state SIBs with a hard carbon anode and a Prussian blue cathode and cycling it at an unprecedented low temperature of ~22 °C for this category of cell chemistry.

4. Experimental section

4.1 Preparation of the polymer electrolyte

The different compositions of the copolymer were synthesized by bulk ring-opening polymerization as described by Mindemark *et al.*[26] The pure poly(ε-caprolactone) (Capa 6500; Perstorp), denoted as 100-0, was stored under inert conditions and used as-received and had a molecular weight of approximately 50 000 g mol^{-1}. This material was dissolved in anhydrous acetonitrile (ACN; Sigma Aldrich, 99.8 %) together with sodium bis(fluorosulfonyl)imide (NaFSI; Solvionic) salt and then cast in PTFE moulds. The ratio of polymer to solvent was 50 mg mL^{-1}. The acetonitrile was carefully evaporated using the same vacuum and heating procedure as described previously.[26] Polymer compositions between 70 and 90 mol% PCL were synthesized, and combined with salt loadings of 10 to 35 wt%.

4.2 Preparation of the electrodes and cell assembly

The anode composite electrode, consisting of 95 wt% hard carbon and 5 wt% CMC-Na (Sigma-Aldrich), was prepared by first ball milling (Retsch Planetary) with deionized water. The slurry was bar-coated (2040 4-sided applicator, Zehntner) on carbon-coated aluminum foil (PI-KEM). The electrodes were dried under vacuum at 120 °C for 12 hours. The cathode composite electrodes, consisting of 85 wt% $Na_xFe[Fe(CN)_6]$ "Prussian blue" (Altris), 5 wt% CMC binder, and 10 wt% CB-C65 (Imerys Graphite and Carbon), were prepared using the same method described above. The capacity of the Prussian blue was 155 mAh g^{-1} according to the supplier, which was also confirmed in a benchmark cell using liquid electrolyte (see Figure S6). All-solid-state Na-ion full cells were built by first infiltration-casting 80-20_{25} dissolved in anhydrous acetonitrile on top of the Prussian blue and hard carbon electrodes. The polymer–salt solution was pre-heated at 40 °C before casting to lower the viscosity and ensure a higher degree of infiltration and wetting. Once the solvent had been removed using the same heating–drying procedure mentioned earlier (see Section 4.1), the stack (12 mm in diameter) was assembled and hermetically sealed in 2025 coin cells. The cells were galvanostatically cycled (BioLogic Science Instruments MPG-2) at 40 °C and at room temperature (~22 °C) between 1.3 and 3.9 V at different current ranges (10 to 120 µA cm^{-2}). All measurements, materials synthesis, and cell assembly involving the polymer electrolytes were carried out under an inert Ar atmosphere.

4.3 Differential Scanning Calorimetry T_g was determined by Differential Scanning Calorimetry (TA Instruments DSC Q2000). Samples were hermetically sealed in aluminium pans and then cooled to −80 °C at −5 °C min^{-1} and then allowed to thermally equilibrate. Next, the samples were heated to 100 °C at 10 °C min^{-1} and then allowed to equilibrate. The cooling and heating procedures were repeated once. The T_g was determined from the inflection point of the step transition using TA Instruments Universal Analysis 2000 V. 4.5A.

The glass transition temperature was obtained from the second cooling–heating cycle to mimic the annealing step prior to ionic conductivity measurements.

4.4 Electrochemical measurements

Total ionic conductivities were determined using Electrochemical Impedance Spectroscopy (Schlumberger Impedance/Gain Phase Analyzer SI 1260). Polymer electrolyte films, 12 mm in diameter and approximately 250 µm in thickness, were hermetically sealed between two blocking electrodes (stainless steel) in 2025 coin cells. The individual thickness of the films was determined using a micrometer (Mitutoyo digital indicator). All samples were annealed at 90 °C (except 100-0, which was annealed at 50 °C) for 1 h and then allowed to cool to room temperature overnight prior to the impedance measurement in order to ensure good contact with the blocking electrodes. The impedance response was measured at a frequency interval from 10 MHz to 1 Hz with an applied amplitude of 10 mV at intervals between 25 to 90 °C. The bulk resistance was determined by fitting a Debye equivalent circuit to the Nyquist plot in the software ZView version 3.2b.[26]

The transference number was measured using the Bruce–Vincent method.[37] Symmetrical cells consisting of a polymer electrolyte film sandwiched between two sodium electrodes were prepared and tested using the same method described previously.[32] The impedance response and chronoamperometric relaxation measurement were done at 80 °C using a portable potentiostat with a EMI-shielded cable (BioLogic SP-240 Potentiostat).

Acknowledgements

This work has been financed through support from the ERC, grant no. 771777 FUN POLYSTORE, and STandUP for Energy. Perstorp AB, Sweden, is acknowledged for the generous gift of poly(ε-caprolactone).

Conflict of interest

R.Y. is co-founder and Research & Development Leader at Altris, a materials technology company focused on commercializing a sodium-based cathode active material, which was used in this study. All other authors declare that they have no competing interests.

Data availability statement

The datasets generated during and/or analyzed during the current study are available from the corresponding author on request.

References

(1) Roth, E. P.; Orendorff, C. J. How Electrolytes Influence Battery Safety. *Interface Mag.* **2012**, *21* (2), 45–49. https://doi.org/10.1149/2.F04122if.

(2) Kalhoff, J.; Eshetu, G. G.; Bresser, D.; Passerini, S. Safer Electrolytes for Lithium-Ion Batteries: State of the Art and Perspectives. *ChemSusChem* **2015**, *8* (13), 2154–2175. https://doi.org/10.1002/cssc.201500284.

(3) Balakrishnan, P. G.; Ramesh, R.; Prem Kumar, T. Safety Mechanisms in Lithium-Ion Batteries. *J. Power Sources* **2006**, *155* (2), 401–414. https://doi.org/10.1016/j.jpowsour.2005.12.002.

(4) Koerver, R.; Aygün, I.; Leichtweiß, T.; Dietrich, C.; Zhang, W.; Binder, J. O.; Hartmann, P.; Zeier, W. G.; Janek, J. Capacity Fade in Solid-State Batteries: Interphase Formation and Chemomechanical Processes in Nickel-Rich Layered Oxide Cathodes and Lithium Thiophosphate Solid Electrolytes. *Chem. Mater.* **2017**, *29* (13), 5574–5582. https://doi.org/10.1021/acs.chemmater.7b00931.

(5) Vikström, H.; Davidsson, S.; Höök, M. Lithium Availability and Future Production Outlooks. *Appl. Energy* **2013**, *110*, 252–266. https://doi.org/10.1016/j.apenergy.2013.04.005.

(6) Vaalma, C.; Buchholz, D.; Weil, M.; Passerini, S. A Cost and Resource Analysis of Sodium-Ion Batteries. *Nat. Rev. Mater.* **2018**, No. 3, 1–11.

(7) Ponrouch, A.; Monti, D.; Boschin, A.; Steen, B.; Johansson, P.; Palacín, M. R. Non-Aqueous Electrolytes for Sodium-Ion Batteries. *J. Mater. Chem. A* **2015**, *3* (1), 22–42. https://doi.org/10.1039/C4TA04428B.

(8) Mogensen, R.; Brandell, D.; Younesi, R. Solubility of the Solid Electrolyte Interphase (SEI) in Sodium Ion Batteries. *ACS Energy Lett.* **2016**, *1* (6), 1173–1178. https://doi.org/10.1021/acsenergylett.6b00491.

(9) West, K. A Rechargeable All-Solid-State Sodium Cell with Polymer Electrolyte. *J. Electrochem. Soc.* **1985**, *132* (12), 3061. https://doi.org/10.1149/1.2113725.

(10) West, K. Sodium Insertion in Vanadium Oxides. *Solid State Ionics* **1988**, *28–30*, 1128–1131. https://doi.org/10.1016/0167-2738(88)90343-8.

(11) Munshi, M. Z. A. Sodium⁄V[Sub 6]O[Sub 13] Polymer Electrolyte Cells. *J. Electrochem. Soc.* **1989**, *136* (6), 1847. https://doi.org/10.1149/1.2097050.

(12) Munshi, M.; Smyrl, W. Insertion Reactions of Sodium in V6O13 Single Crystals from a Solid Polymeric Electrolyte. *Solid State Ionics* **1991**, *45* (3–4), 183–189. https://doi.org/10.1016/0167-2738(91)90151-Z.

(13) Doeff, M. M.; Peng, M. Y.; Ma, Y.; De Jonghe, L. C. Orthorhombic Na[Sub x]MnO[Sub 2] as a Cathode Material for Secondary Sodium and Lithium Polymer Batteries. *J. Electrochem. Soc.* **1994**, *141* (11), L145–L147. https://doi.org/10.1149/1.2059323.

(14) Doeff, M. M.; Ferry, A.; Ma, Y.; Ding, L.; De Jonghe, L. C. Effect of Electrolyte Composition on the Performance of Sodium/Polymer Cells. *J. Electrochem. Soc.* **1997**, *144* (2), L20–L22. https://doi.org/10.1149/1.1837419.

(15) Colò, F.; Bella, F.; Nair, J. R.; Destro, M.; Gerbaldi, C. Cellulose-Based Novel Hybrid Polymer Electrolytes for Green and Efficient Na-Ion Batteries. *Electrochim. Acta* **2015**, *174*, 185–190. https://doi.org/10.1016/j.electacta.2015.05.178.

(16) Qi, X.; Ma, Q.; Liu, L.; Hu, Y.-S.; Li, H.; Zhou, Z.; Huang, X.; Chen, L. Sodium Bis(Fluorosulfonyl)Imide/Poly(Ethylene Oxide) Polymer Electrolytes for Sodium-Ion Batteries. *ChemElectroChem* **2016**, *3* (11), 1741–1745. https://doi.org/10.1002/celc.201600221.

(17) Ma, Y.; Doeff, M. M.; Visco, S. J.; De Jonghe, L. C. Rechargeable Na/$Na_xCoO_2$and $Na_{15}Pb_4$/Na_xCoO_2 Polymer Electrolyte Cells. *J. Electrochem. Soc.* **1993**, *140* (10), 2726–2732. https://doi.org/10.1149/1.2220900.
(18) Cherng, J. Y.; Munshi, M. Z. A.; Owens, B. B.; Smyrl, W. H. Applications of Multivalent Ionic Conductors to Polymeric Electrolyte Batteries. *Solid State Ionics* **1988**, *28–30*, 857–861. https://doi.org/10.1016/S0167-2738(88)80159-0.
(19) Koksbang, R.; Yde-Andersen, S.; West, K.; Zachau-Christiansen, B.; Skaarup, S. Lithium and Sodium Insertion in Ternary Chromium Oxides. *Solid State Ionics* **1988**, *28–30*, 868–872. https://doi.org/10.1016/S0167-2738(88)80161-9.
(20) Ma, Q.; Liu, J.; Qi, X.; Rong, X.; Shao, Y.; Feng, W.; Nie, J.; Hu, Y.-S.; Li, H.; Huang, X.; et al. A New Na[(FSO_2)(n-$C_4F_9SO_2$)N]-Based Polymer Electrolyte for Solid-State Sodium Batteries. *J. Mater. Chem. A* **2017**, *5* (17), 7738–7743. https://doi.org/10.1039/C7TA01820G.
(21) Mindemark, J.; Mogensen, R.; Smith, M. J.; Silva, M. M.; Brandell, D. Polycarbonates as Alternative Electrolyte Host Materials for Solid-State Sodium Batteries. *Electrochem. Commun.* **2017**, *77*, 58–61. https://doi.org/10.1016/j.elecom.2017.02.013.
(22) Zhao, C.; Liu, L.; Qi, X.; Lu, Y.; Wu, F.; Zhao, J.; Yu, Y.; Hu, Y.-S.; Chen, L. Solid-State Sodium Batteries. *Adv. Energy Mater.* **2018**, *8* (17), 1703012. https://doi.org/10.1002/aenm.201703012.
(23) Mindemark, J.; Sun, B.; Törmä, E.; Brandell, D. High-Performance Solid Polymer Electrolytes for Lithium Batteries Operational at Ambient Temperature. *J. Power Sources* **2015**, *298*, 166–170. https://doi.org/10.1016/j.jpowsour.2015.08.035.
(24) Xue, Z.; He, D.; Xie, X. Poly(Ethylene Oxide)-Based Electrolytes for Lithium-Ion Batteries. *J. Mater. Chem. A* **2015**, *3* (38), 19218–19253. https://doi.org/10.1039/C5TA03471J.
(25) Mindemark, J.; Lacey, M.; Bowden, T.; Brandell, D. Beyond PEO—Alternative Host Materials for Li+-Conducting Solid Polymer Electrolytes. *Prog. Polym. Sci.* **2018**, No. 81, 114–143. https://doi.org/https://doi.org/10.1016/j.progpolymsci.2017.12.004.
(26) Mindemark, J.; Törmä, E.; Sun, B.; Brandell, D. Copolymers of Trimethylene Carbonate and ε-Caprolactone as Electrolytes for Lithium-Ion Batteries. *Polymer* **2015**, *63*, 91–98. https://doi.org/10.1016/j.polymer.2015.02.052.
(27) Le Nest, J. F.; Gandini, A.; Cheradame, H.; Cohen-Addad, J. P. Influence of Lithium Perchlorate on the Properties of Polyether Networks: Specific Volume and Glass Transition Temperature. *Macromolecules* **1988**, *21* (4), 1117–1120. https://doi.org/10.1021/ma00182a044.
(28) Mao, G.; Perea, R. F.; Howells, W. S.; Price, D. L.; Saboungi, M.-L. Relaxation in Polymer Electrolytes on the Nanosecond Timescale. *Nature* **2000**, *405* (6783), 163–165. https://doi.org/10.1038/35012032.
(29) Sun, B.; Mindemark, J.; Edström, K.; Brandell, D. Polycarbonate-Based Solid Polymer Electrolytes for Li-Ion Batteries. *Solid State Ionics* **2014**, *262*, 738–742. https://doi.org/10.1016/j.ssi.2013.08.014.
(30) Sun, B.; Mindemark, J.; V. Morozov, E.; Costa, L. T.; Bergman, M.; Johansson, P.; Fang, Y.; Furó, I.; Brandell, D. Ion Transport in Polycarbonate Based Solid Polymer Electrolytes: Experimental and Computational Investigations. *Phys. Chem. Chem. Phys.* **2016**, *18* (14), 9504–9513. https://doi.org/10.1039/C6CP00757K.
(31) Åvall, G.; Mindemark, J.; Brandell, D.; Johansson, P. Sodium-Ion Battery Electrolytes: Modeling and Simulations. *Adv. Energy Mater.* **2018**, *8* (17), 1703036. https://doi.org/10.1002/aenm.201703036.

(32) Sångeland, C.; Mogensen, R.; Brandell, D.; Mindemark, J. Stable Cycling of Sodium Metal All-Solid-State Batteries with Polycarbonate-Based Polymer Electrolytes. *Accepted for publication in ACS Applied Polymer Materials*.
(33) Eriksson, T.; Mindemark, J.; Yue, M.; Brandell, D. Effects of Nanoparticle Addition to Poly(ε-Caprolactone) Electrolytes: Crystallinity, Conductivity and Ambient Temperature Battery Cycling. *Electrochim. Acta* **2019**, *300*, 489–496. https://doi.org/10.1016/j.electacta.2019.01.117.
(34) Teran, A. A.; Tang, M. H.; Mullin, S. A.; Balsara, N. P. Effect of Molecular Weight on Conductivity of Polymer Electrolytes. *Solid State Ionics* **2011**, *203* (1), 18–21. https://doi.org/10.1016/j.ssi.2011.09.021.
(35) Timachova, K.; Watanabe, H.; Balsara, N. P. Effect of Molecular Weight and Salt Concentration on Ion Transport and the Transference Number in Polymer Electrolytes. *Macromolecules* **2015**, *48* (21), 7882–7888. https://doi.org/10.1021/acs.macromol.5b01724.
(36) Bhide, A.; Hofmann, J.; Katharina Dürr, A.; Janek, J.; Adelhelm, P. Electrochemical Stability of Non-Aqueous Electrolytes for Sodium-Ion Batteries and Their Compatibility with $Na_{0.7}CoO_2$. *Phys. Chem. Chem. Phys.* **2014**, *16* (5), 1987–1998. https://doi.org/10.1039/C3CP53077A.
(37) Evans, J.; Vincent, C. A.; Bruce, P. G. Electrochemical Measurement of Transference Numbers in Polymer Electrolytes. *Polymer* **1987**, *28* (13), 2324–2328. https://doi.org/10.1016/0032-3861(87)90394-6.
(38) Devaux, D.; Bouchet, R.; Glé, D.; Denoyel, R. Mechanism of Ion Transport in PEO/LiTFSI Complexes: Effect of Temperature, Molecular Weight and End Groups. *Solid State Ionics* **2012**, *227*, 119–127. https://doi.org/10.1016/j.ssi.2012.09.020.
(39) Wang, L.; Song, J.; Qiao, R.; Wray, L. A.; Hossain, M. A.; Chuang, Y.-D.; Yang, W.; Lu, Y.; Evans, D.; Lee, J.-J.; Vail, S.; Xin, Z.; Motoaki, N.; Seizoh, K.; Goodenough, J.B. Rhombohedral Prussian White as Cathode for Rechargeable Sodium-Ion Batteries. *J. Am. Chem. Soc.* **2015**, *137* (7), 2548–2554. https://doi.org/10.1021/ja510347s.
(40) You, Y.; Wu, X.-L.; Yin, Y.-X.; Guo, Y.-G. High-Quality Prussian Blue Crystals as Superior Cathode Materials for Room-Temperature Sodium-Ion Batteries. *Energy Environ. Sci.* **2014**, *7* (5), 1643–1647. https://doi.org/10.1039/C3EE44004D.
(41) Bommier, C.; Leonard, D.; Jian, Z.; Stickle, W. F.; Greaney, P. A.; Ji, X. New Paradigms on the Nature of Solid Electrolyte Interphase Formation and Capacity Fading of Hard Carbon Anodes in Na-Ion Batteries. *Adv. Mater. Interfaces* **2016**, *3* (19), 1600449. https://doi.org/10.1002/admi.201600449.
(42) Hiller, M. M.; Joost, M.; Gores, H. J.; Passerini, S.; Wiemhöfer, H.-D. The Influence of Interface Polarization on the Determination of Lithium Transference Numbers of Salt in Polyethylene Oxide Electrolytes. *Electrochim. Acta* **2013**, *114*, 21–29. https://doi.org/10.1016/j.electacta.2013.09.138.

Supplementary Information

Towards room temperature operation of all-solid-state Na-ion batteries through polyester–polycarbonate-based polymer electrolytes

Differential Scanning Calorimetry curves

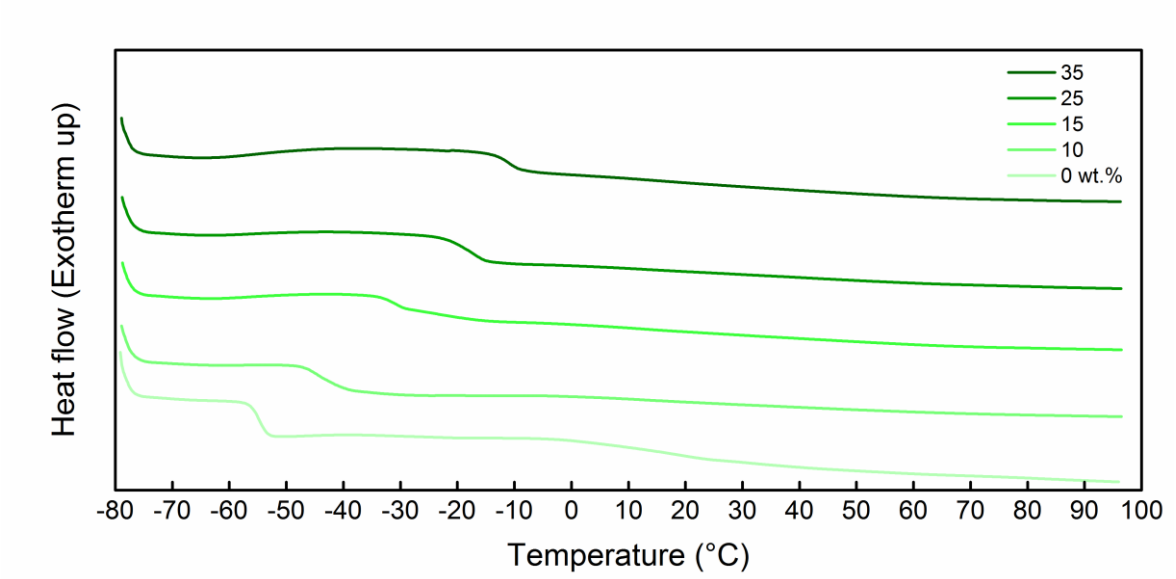

Figure S1: DSC heating scans of PCL_{70}-$PTMC_{30}$ with different NaFSI salt concentrations.

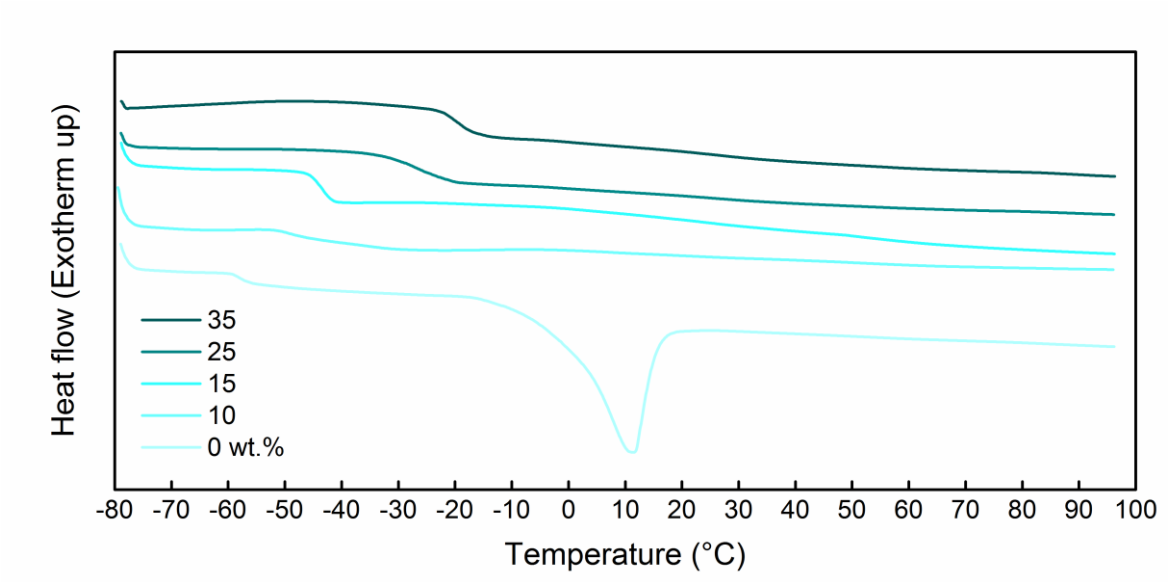

Figure S2: DSC heating scans of PCL_{80}-$PTMC_{20}$ with different NaFSI salt concentrations.

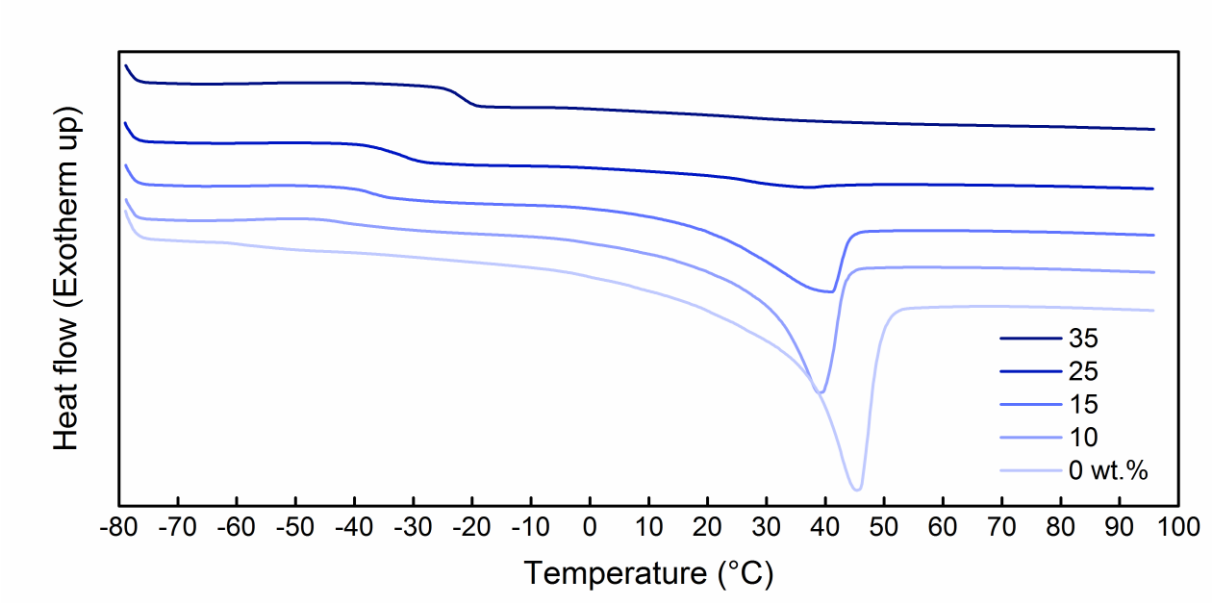

Figure S3: DSC heating scans of PCL_{90}-$PTMC_{10}$ with different NaFSI salt concentrations.

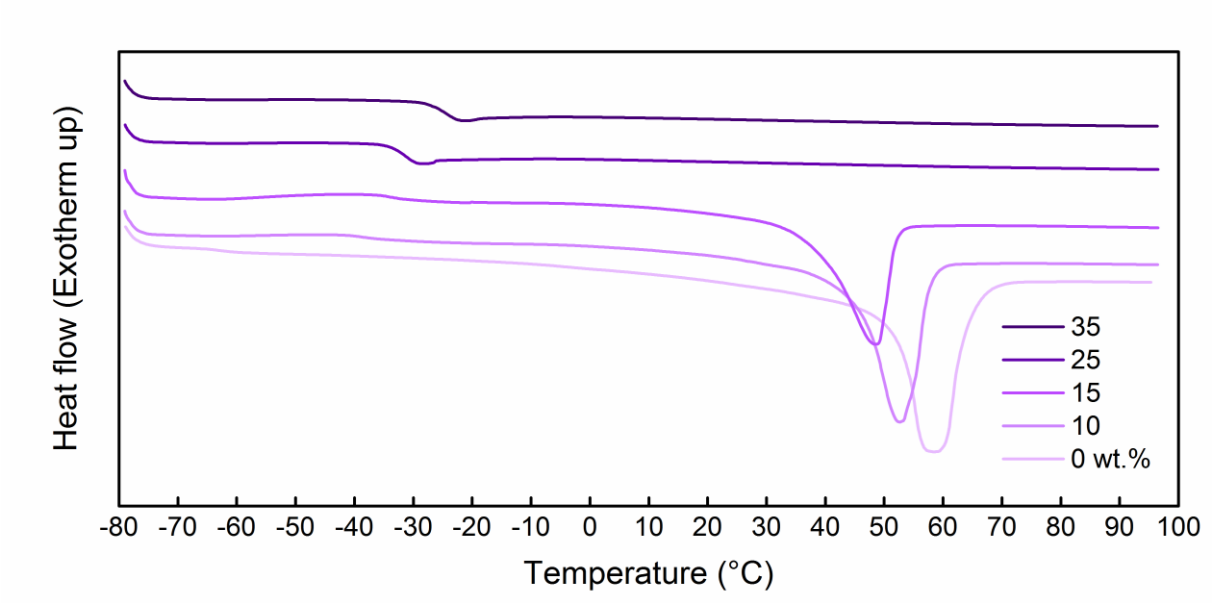

Figure S4: DSC heating scans of PCL_{100}-$PTMC_{0}$ with different NaFSI salt concentrations.

Total ionic conductivity measurements

The Vogel-Fulcher-Tammann (VFT) equation (Equation S1) describes the relationship between total ionic conductivity and temperature in amorphous polymer electrolytes.

$$\sigma = \frac{A}{\sqrt{T}} e^{-\frac{B}{T-T_0}} \quad \text{(S1)}$$

Table S1: Values obtained for parameters in the fitted VFT Equation.

Composition [PCL–PTMC mol %]	**NaFSI concentration** [wt%]	***A*** [S cm^{-1} K$^{1/2}$]	***B*** [K]	T_0 [K]
70-30	10	8.43795	1484.31621	167.91777
70-30	15	4.97276	1230.73361	187.02848
70-30	25	32.05162	1573.15661	185.74773
70-30	35	1.04059	1164.95092	212.77002
80-20	10	23.5094	1612.02842	158.67419
80-20	15	5.99841	1142.82259	190.75194
80-20	25	5.17854	991.87961	209.3695
80-20	35	13.29105	1104.37357	208.85581
90-10	10	1.47719	723.38644	228.25352
90-10	15	7.64838	1138.78953	197.30493
90-10	25	13.83188	1379.3505	183.85169
90-10	35	11.71288	1022.58884	216.87239
100-0	10	1.10595*	570.57022*	237.13314*
100-0	15	2.57909*	719.5838*	212.91315*
100-0	25	0.92707	540.48431	231.13254
100-0	35	1.15888	494.8637	238.44586

* VFT fitting was only applied for data points above T_m.

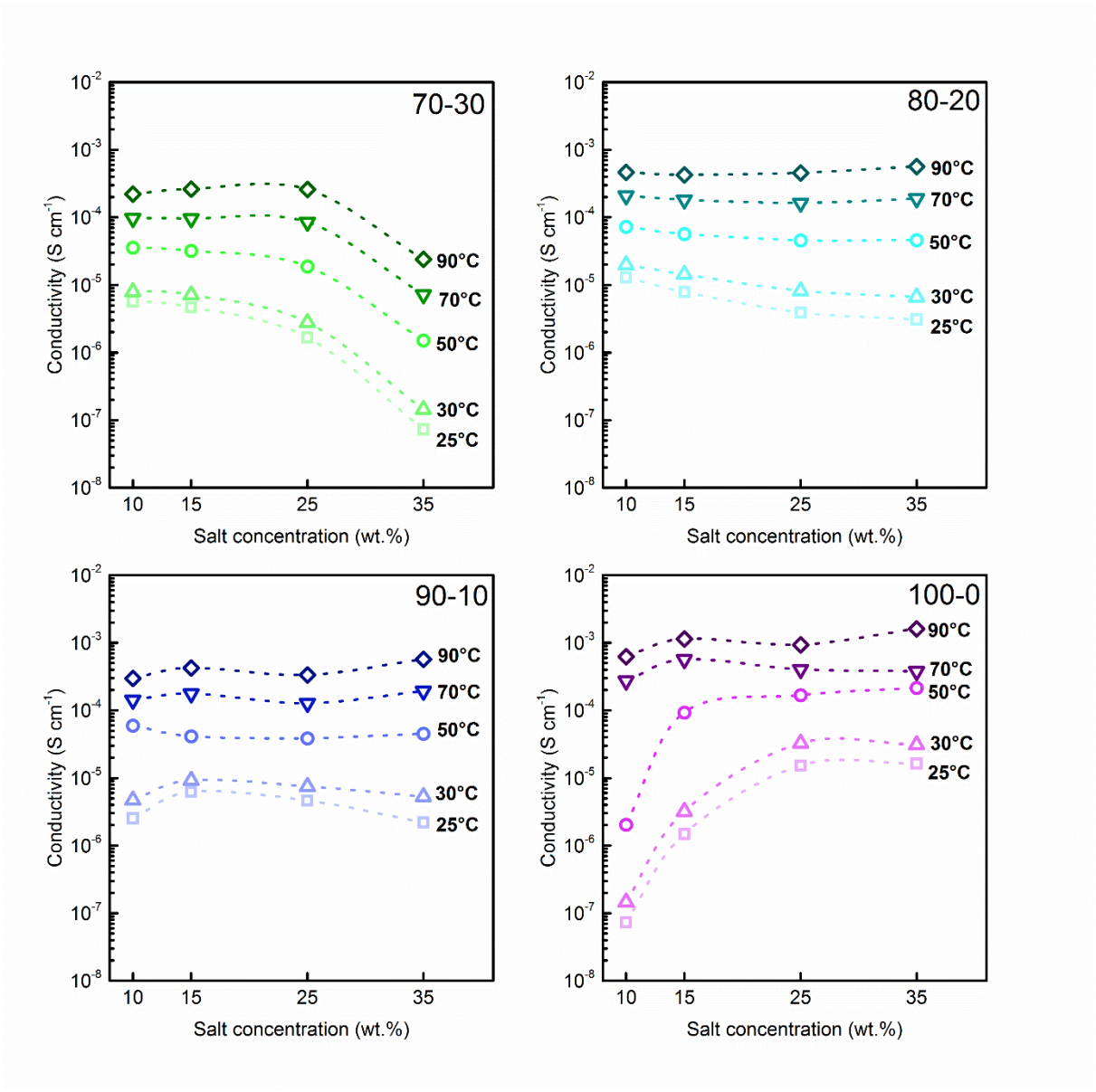

Figure S5: Total ionic conductivity isotherms for PCL_{100-x}-$PTMC_x$ (x=0, 10, 20, and 30) with different NaFSI salt concentrations.

Table S2: Total ionic conductivity for PCL_{100-x}-$PTMC_x$ (x=0, 10, 20, and 30) with different NaFSI salt concentrations at 25 and 80 °C.

Composition [PCL–PTMC mol %]	**NaFSI concentration** [wt%]	**Conductivity at 25 °C** [S cm^{-1}]	**Conductivity at 80 °C** [S cm^{-1}]
70-30	10	5.72×10^{-6}	1.47×10^{-4}
70-30	15	4.66×10^{-6}	1.65×10^{-4}
70-30	25	1.66×10^{-6}	1.38×10^{-4}
70-30	35	7.30×10^{-8}	1.38×10^{-5}
80-20	10	1.29×10^{-5}	3.09×10^{-4}
80-20	15	7.85×10^{-6}	2.75×10^{-4}
80-20	25	3.90×10^{-6}	2.73×10^{-4}
80-20	35	3.08×10^{-6}	3.32×10^{-4}
90-10	10	2.53×10^{-6}	2.13×10^{-4}
90-10	15	6.17×10^{-6}	2.95×10^{-4}
90-10	25	4.60×10^{-6}	2.12×10^{-4}
90-10	35	2.19×10^{-6}	3.50×10^{-4}
100-0	10	7.26×10^{-8}	4.37×10^{-4}
100-0	15	1.48×10^{-6}	7.95×10^{-4}
100-0	25	1.52×10^{-6}	5.44×10^{-4}
100-0	35	1.64×10^{-5}	6.54×10^{-4}

The transference number

The Bruce-–Vincent equation (see Equation S2) was used to calculate the transference number T^+ from the applied potentiostatic bias (ΔV), the current at steady-state (I_s), the initial current (I_0), the initial polymer-electrolyte interfacial resistance ($R_{\text{int }0}$), and the polymer-electrolyte interface resistance at steady-state ($R_{\text{int S}}$).

$$T^+ = \frac{I_s(\Delta V - I_0 R_{\text{int }0})}{I_0(\Delta V - I_s R_{\text{int S}})} \quad \text{(S2)}$$

The resistances of the polymer-electrode interfaces before and after polarization were obtained by fitting the equivalent circuit seen in Figure S6 to the Nyquist plot.

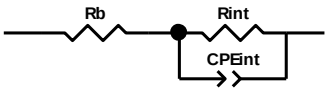

Figure S6: Equivalent circuit simulating the bulk electrolyte ionic resistance (Rb), the ionic resistance of the electrode–electrolyte interface (Rint), and the capacitance of the electrode–electrolyte interface (CPEint).

Finally, the initial current (I_0) was calculated using Equation S3 as demonstrated by Hiller *et al.*[42] Using Ohm's law, the initial current (I_0) is calculated using the applied potential (ΔV), the initial ionic resistance of the bulk electrolyte ($R_{\text{b }0}$), and the initial polymer–electrolyte interfacial resistance ($R_{\text{int }0}$).

$$I_0 = \frac{\Delta V}{R_{\text{b }0} + R_{\text{int }0}} \quad \text{(S3)}$$

The values inserted into Equation S2 to calculate the transference number can be seen in Table S2.

Table S3: The obtained values which were inserted into the Bruce−Vincent equation to calculate the transference number.

Parameter	Value
$R_{b\,0}$	16.00 Ω
$R_{int\,0}$	55.51 Ω
$R_{int\,S}$	60.91 Ω
I_0	139.84 µA
I_s	105.55 µA

Cycling of benchmark cell with liquid electrolyte at room temperature

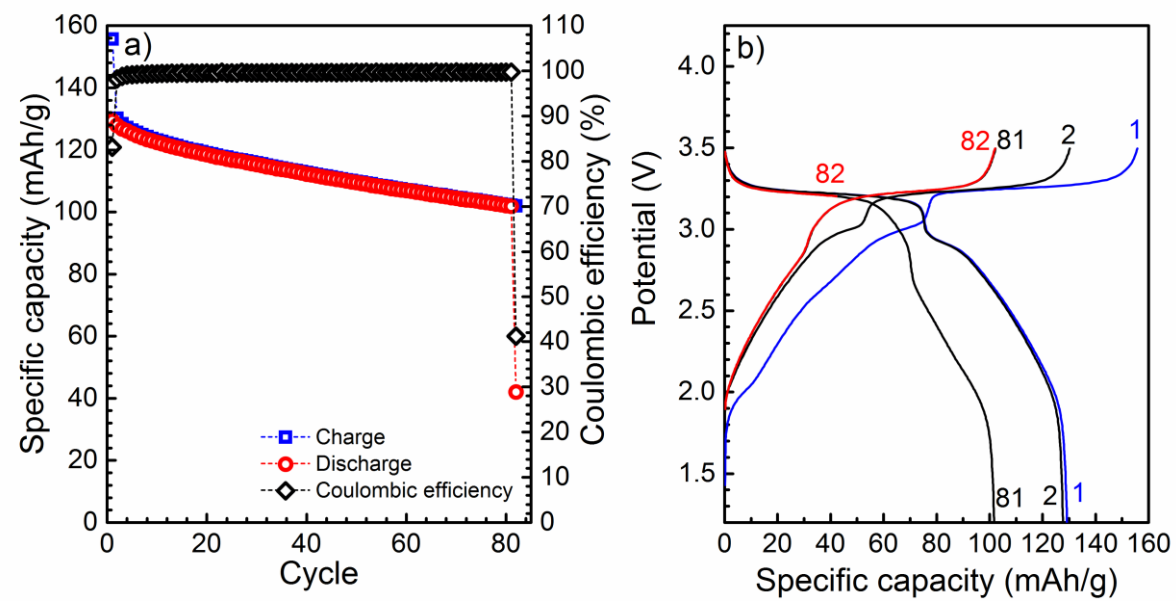

Figure S6: a) Charge and discharge capacity and columbic efficiency per cycle and b) voltage profiles for Prussian blue and hard carbon with 1 M $NaPF_6$ in EC:DEC (1:1 v/v) , cycled at 23.0 °C at 10 µA cm^{-2}. The areal cathode composite mass loading was 2.00 mg cm^{-2}.

Carbonyl–sodium ion coordination

Sun *et al.* have previously shown that Li^+ has a preferential coordination to the carbonyl oxygen in the ester group rather than the carbonyl oxygen in the carbonate group.[30] To see if the same behavior could be observed with NaFSI, the PCL–PTMC:NaFSI system was analyzed using Fourier Transform Infrared Spectroscopy. Polymer films with and without NaFSI salt were analyzed in Attenuated Total Reflection mode (Bruker Alpha FT-IR spectrometer with diamond crystal). Each spectrum was taken from 3200 to 400 cm^{-1} with a total of 300 scans and 2 cm^{-1} resolution. The data was analyzed using Origin 2016 where a linear baseline was first subtracted followed by normalization and peak fitting. Unfortunately, as seen in Figure S7 below, the peak arising from the coordinating carbonyl in PTMC (0-100_{25}) overlapped with the carbonyl peak in the pure PCL (100-0_0). This meant that it was not possible to deconvolute the PCL–PTMC:NaFSI spectra. The results do, however, indicate that the carbonyl stretch is broader or less affected by the sodium ion compared to lithium where the carbonyl peak was clearly split into two separate contributions.[30]

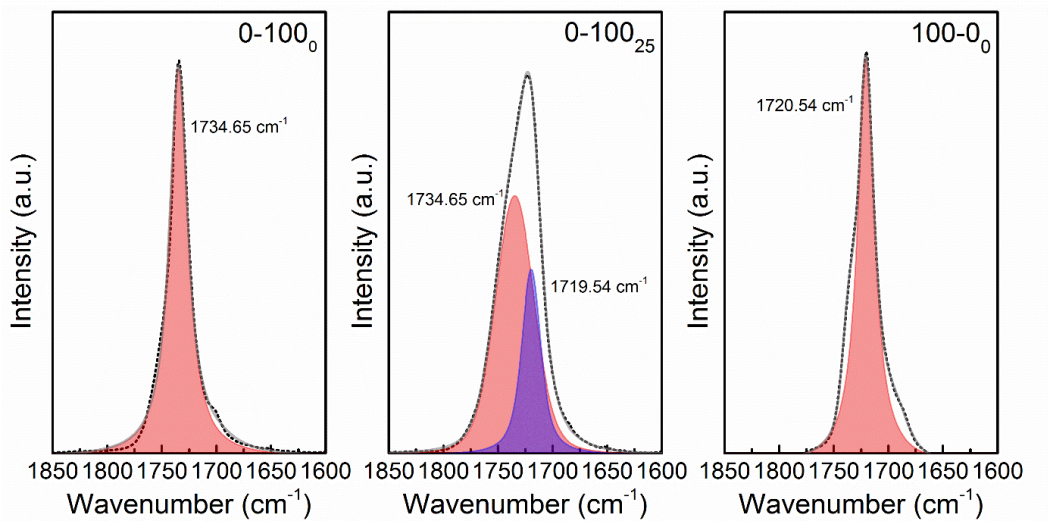

Figure S7: Deconvoluted FTIR spectra (Voigtian lineshapes) of a) 0-100_0, b) 0-100_{25}, and c) 100-0 between 1850 and 1600 cm^{-1} showing the carbonyl stretch. Experimental data is shown in black dotted lines, the red peaks indicate the uncoordinated carbonyl, the blue peak indicate the coordinated carbonyl, and the cumulative fit is shown in gray solid lines. The annotated numbers correspond to peak centers.

Cycling of HC|80-20$_{10}$|Na$_{2-x}$Fe(Fe(CN)$_6$) cell at room temperature

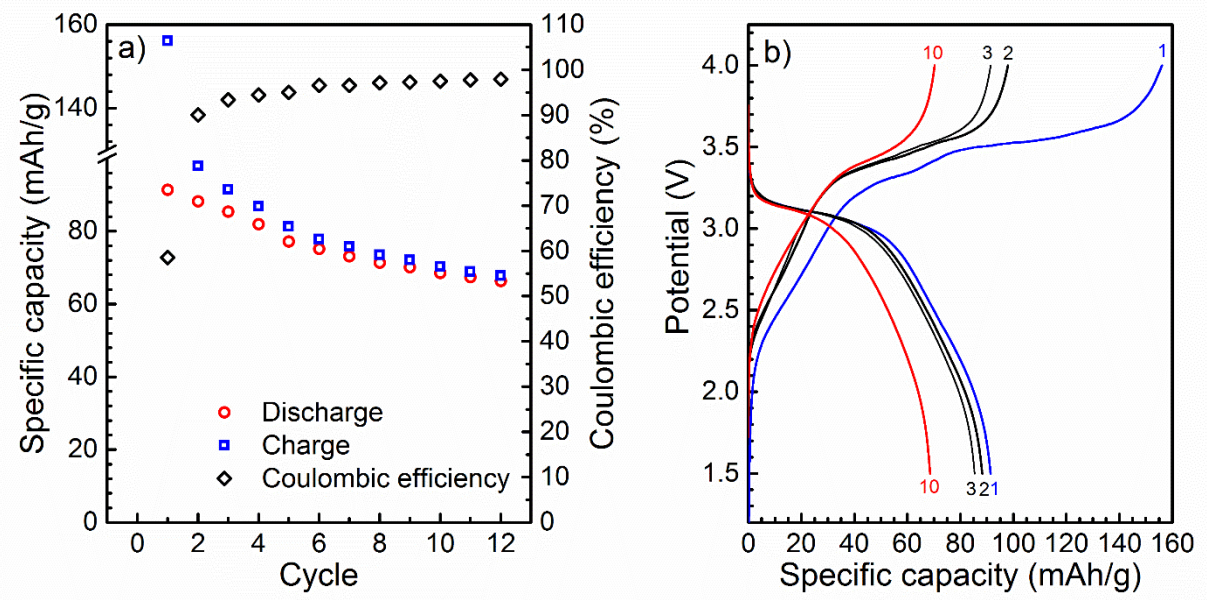

Figure S8: a) Charge and discharge capacity and coulombic efficiency per cycle and b) voltage profiles for HC|80-20$_{10}$|Na$_{2-x}$Fe(Fe(CN)$_6$) cycled at ~22 °C and 10 µA cm^{-2}.